Adaptive optimization on ultrasonic transmission tomography-based temperature image for biomedical treatment*

Yun-Hao Zhu(朱昀浩)[1], Jie Yuan(袁杰)[1,†], Stephen Z Pinter[2], Oliver D Kripfgans[2], Qian Cheng(程茜)[4], Xue-Ding Wang(王学鼎)[4], Chao Tao(陶超)[3], Xiao-Jun Liu(刘晓峻)[3], Guan Xu(徐冠)[2], and Paul L Carson[2]

[1] *School of Electronic Science and Engineering, Nanjing University, Nanjing* 210093, *China*
[2] *Department of Radiology, University of Michigan, Ann Arbor, MI, USA*
[3] *School of Physics, Nanjing University, Nanjing* 210093, *China*
[4] *School of Physics, Tongji University, Shanghai* 200092, *China*

(Received 6 December 2016; revised manuscript received 9 March 2017; published online 20 April 2017)

Hyperthermia has proven to be beneficial to treating superficial malignancies, particularly chest wall recurrences of breast cancer. During hyperthermia, monitoring the time–temperature profiles in the target and surrounding areas is of great significance for the effect of therapy. An ultrasound-based temperature imaging method has advantages over other approaches. When the temperature around the tumor is calculated by using the propagation speed of ultrasound, there always exist overshoot artifacts along the boundary between different tissues. In this paper, we present a new method combined with empirical mode decomposition (EDM), similarity constraint, and continuity constraint to optimize the temperature images. Simulation and phantom experiment results compared with those from our previously proposed method prove that the EMD-based method can build a better temperature field image, which can adaptively yield better temperature images with less computation for assistant medical treatment control.

Keywords: temperature imaging, empirical mode decomposition, ultrasound transmission tomography

PACS: 43.35.Wa, 43.80.Sh, 81.70.Cv **DOI:** 10.1088/1674-1056/26/6/064301

1. Introduction

Hyperthermia is proved to be beneficial to treating chest wall recurrences of breast cancer.[1–4] Researches have proved that the combination of hyperthermia and other medical treatments, especially radiotherapy in local control[5,6] and chemotherapy,[7,8] can yield better medical effects. In order to achieve the best treatment effect in hyperthermia, temperature ranges in the target area are typically tuned close to 42 °C or 43 °C ±1 °C. Therefore, precisely monitoring temperature is of great importance to assure safe medical treatment.

Invasive temperature measurement methods have been used primarily by embedding heat-sensitive sensors in the tissues. These methods give accurate local results, low cost, and easy operation. However, spatial sampling is too limited to make corrections for most of the tissue heterogeneities in a complex tissue like breast and it brings pain and risk of infection to the patient.[9] Common medical measurement methods with non-invasive attributes have previously been studied including: magnetic resonance (MR),[10,11] ultrasound,[12,13] and microwave[14] technologies. The three-dimensional (3D) temperature imaging with MR methods based on the diffusion coefficient,[15] the relaxation time, or proton resonance frequency (PRF)[16] of tissue has also been well reported. A hybrid PRF approach to simultaneously measuring time variations of PRF shift temperatures in water-based tissue and in fat-based tissues is proposed,[17] which makes temperature changes accurately monitored in both water-based and fat-based tissues. However, it costs quite a lot in the cycle of multiple treatments when the MR method is reused. While a temperature measurement method based on microwaves has proved that the microwave can penetrate into tissue in only a limited depth and can be easily influenced by the environment.[18] Ultrasound is a convenient, non-ionizing, and inexpensive method with less calculation requirements for temperature monitoring. The methods of using ultrasound as a temperature monitor involve measuring the sound attenuation coefficient,[19,20] measuring echo-shift deviation in tissue thermal expansion,[21,22] and measuring the backscattered energy difference of tissue in homogeneities.[23] Several research centers in the world are working on constructing a prototype of ultrasonic transmission tomography for women's breast examination. In our experiment, a clinical ultrasound ring array scanner for breast cancer diagnosis was built to record both reflected ultrasound energy and transmitted ultrasound energy.[24,25] However, the prior information about propagation speed of ultrasound and coefficient of thermal expansion are necessary for the echo-shift method.[26]

*Project supported by the DoD/BCRP Idea Award BC095397P1, the National Natural Science Foundation of China (Grant No. 61201425), and the Priority Academic Program Development of Jiangsu Higher Education Institutions, China.

†Corresponding author. E-mail: yuanjie@nju.edu.cn

© 2017 Chinese Physical Society and IOP Publishing Ltd

Maintaining uniform temperature over one or more large target regions requires the compensation for a number of factors. The Pennes bioheat equation[27,28] allows fairly good calculation provided that each of these variables is reasonably a function of time, but it is not so easy to determine the values of these factors for hyperthermia treatments and measurements as required. Some of these factors, particularly perfusion and absorption coefficients are substantially different in different tissues. Therefore, temperature often changes rapidly near tissue boundaries. This phenomenon will inevitably be wrongly reflected as overshoot artifacts around tissue boundaries, such as the greatly different thermal coefficients of speed of ultrasound between fat and muscle or connective tissues, when building temperature images with ultrasonic transmission tomography.

Researches on reducing overshoot artifacts normally consider the root cause of the artifacts and then perform an inverse operation.[29,30] Our previous contribution[31] proposed a method based on a physical mode. When applying our previous method, we solve a differential equation based on heat conduction rules with boundary conditions. Although the result is satisfactory for future biomedical treatment, it is characterized with a heavy computation burden and lack of the adaptive property.

In this paper, an alternative method of combining deconvolution, continuity constraint and empirical mode decomposition (EMD)[32,33] is proposed to build a temperature image based on ultrasonic transmission speed tomography, which can yield better border information adaptively with less calculation. The proposed method can provide accurate and fast measurements for assistant medical treatment control by effectively alleviating the negative effect from overshoot artifacts in temperature images. The rest of this paper is organized as follows. In Section 2, both the direct method and the proposed method of optimally rebuilding the temperature image are presented. In Section 3, the experimental result and the analysis are given for subjective evaluation. Finally, conclusions are given in Section 4.

2. Methods

2.1. EMD

EMD, introduced by Huang *et al.*,[33] is an excellent data analysis method for non-stationary signals. The kernel of EMD is to decompose a signal into a group of intrinsic mode functions (IMF), which are the fundamental representing of the signal. As the decomposition process is adaptive, the EMD is especially suitable for analyzing signals with nonlinear or non-stationary properties.[34] An IMF must satisfy two requirements. The first one is that the number of zero crossings and the number of extreme points should differ by no more than one. The second one is the local average, which is normally equal to the mean of the maximum and minimum envelopes around the signal, obtained by using cubic spline interpolation through the corresponding local extrema, and must be zero.

2.2. Imaging

2.2.1. Ultrasound-based temperature imaging

With an ultrasound transmission speed image and the profiles between the speed of sound and temperature for different homogeneous tissues, we can build a basic temperature image. As for each homogeneous tissue, which can be segmented from the speed of sound image, we can calculate temperature from these profiles directly. While for the mixture area between two tissues, on the assumption that multi-scattering is neglected, the relationship between the transmission ultrasound speed and temperature can be expressed as a linear transition between these two tissues.

To refine the speed of sound image segmentation in the mixture area, homogeneous areas, and the corresponding mixture area are separated by the following rule:

$$(x,y) \in \begin{cases} \text{tissue}_1, & v(x,y) \le v_1, \\ \text{tissue}_2, & v(x,y) \ge v_2, \\ \text{mixture area}, & \text{else}, \end{cases} \tag{1}$$

$$v_n = \frac{\int_{S_n} v(x,y)\,\mathrm{d}S}{S_n}, (x,y) \in \text{tissue}_n, \quad n = 1,2, \tag{2}$$

where $v(x,y)$ is the propagation speed of sound on the x–y plane, v_1 and v_2 are the average sound propagation speeds in tissue$_1$ and tissue$_2$ respectively, S_n $(n = 1,2)$ are the homogeneous areas of tissue$_1$ and tissue$_2$ respectively and we suppose $v_1 < v_2$.

With the profiles between the speed of sound versus temperature in tissue$_1$ and tissue$_2$, temperature in a homogeneous tissue area can be acquired through

$$T_1 = f_1(v), T_2 = f_2(v). \tag{3}$$

where $f_1(v)$ and $f_2(v)$ are the relationships between temperature and speed of ultrasound in tissue$_1$ and tissue$_2$ respectively.

The propagation speed of sound in the mixture area of two homogeneous tissues is a multi-variable function caused by factors like the applied intensity absorption, the distribution of metabolic heat generation, heat conduction in the tissues, heat convection by flowing blood, heat loss by radiation, convection, and evaporation at the surface, and heat exchange between veins and arteries. Although the mapping from speed of sound to temperature in the mixture area is a multi-variable function, we can still simplify it by a linear interpolation PSF since the thickness of the mixture area is relatively small compared with that of the homogeneous area. Then, we can obtain

$$\begin{aligned} v'(x,y) \;=\; & v(x_1,y_1) + (v(x_2,y_2) - v(x_1,y_1)) \\ & \cdot \frac{x-x_1}{\Delta x} \cdot \frac{y-y_1}{\Delta y} \Bigg|_{(x_1,y_1)}^{(x_2,y_2)}, \end{aligned} \tag{4}$$

where $\Delta x = x_1 - x_2$ and $\Delta y = y_1 - y_2$. (x_n, y_n) $(n = 1, 2)$ denotes the thickness of the mixture area. Rewrite Eq. (4) as

$$v'(x,y) = \left(1 - \frac{(x-x_1)(y-y_1)}{(x_2-x_1)(y_2-y_1)}\right)\Bigg|_{(x_1,y_1)}^{(x_2,y_2)} \cdot v(x_1,y_1) + \frac{(x-x_1)(y-y_1)}{(x_2-x_1)(y_2-y_1)}\Bigg|_{(x_1,y_1)}^{(x_2,y_2)} \cdot v(x_2,y_2). \quad (5)$$

Substituting Eq. (3) into Eq. (5), the temperature in the mixture area can be expressed as

$$T'(x,y) = \left(1 - \frac{(x-x_1)(y-y_1)}{(x_2-x_1)(y_2-y_1)}\right)\Bigg|_{(x_1,y_1)}^{(x_2,y_2)} \cdot T(x_1,y_1) + \frac{(x-x_1)(y-y_1)}{(x_2-x_1)(y_2-y_1)}\Bigg|_{(x_1,y_1)}^{(x_2,y_2)} \cdot T(x_2,y_2), \quad (6)$$

where T' is the temperature in the mixture area. Suppose that a low-temperature homogeneous tissue is surrounded by homogenous tissue with high temperature, when the mixture areas are correctly segmented and Eqs. (3)–(5) are correctly applied, we can reach a good result as denoted by the blue curve in Fig. 1. However, when the boundary is unknown, the mixture area is inevitably blurred by Eqs. (1) and (2). After equation (6) is employed in the mixture area, the artifacts are illustrated as shown by the red curve in Fig. 1. The overshoot of temperature in the transitional area is abnormal.

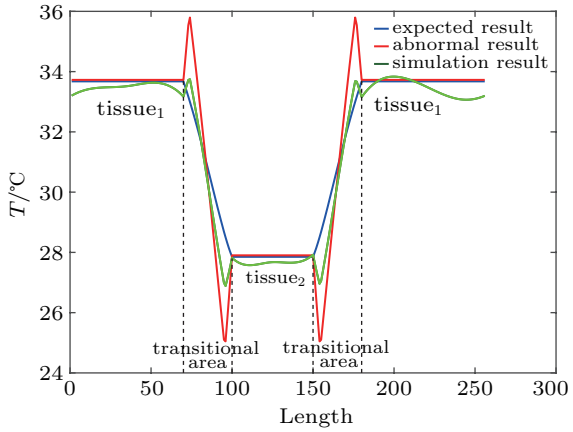


Fig. 1. (color online) Illustration of overshoot artifacts.

2.2.2. Proposed optimized imaging method

Since the EMD is characterized with an adaptive property for a non-stationary signal, the IMFs from the temperature EMD reflect the versatile intrinsic relationship between the ground truth values and artifacts. Thus, attaching a proper weight coefficient on each IMF and reconstructing it under different constraint can yield a signal similar to that applied to a certain filter.[35] In this contribution, after building the weight coefficient through ultrasonic transmission tomography, we adopt EMD on the temperature image without its DC component to generate IMF and then adaptively select the weight coefficient under continuity and similarity constraints for image optimization. The method is described in detail as follows.

Step 1 Apply EMD to one row/column un-optimized, temperature signal $\text{origin}(n)$, $n = 1, \ldots, N$ without DC component and obtain its IMF:

$$\text{origin}(n) = \sum_k \text{IMF}_k + r(n). \quad (7)$$

Step 2 Use a coefficient matrix to reconstruct a set of candidate temperature $\text{new}_i(n)$ $(i = 1, \ldots, l)$:

$$\begin{bmatrix} \text{new}_1(n) \\ \text{new}_2(n) \\ \vdots \\ \text{new}_l(n) \end{bmatrix} = \begin{bmatrix} a_{11} & a_{12} & \ldots & a_{1k}1 \\ a_{21} & a_{22} & \ldots & a_{2}1 \\ \vdots & \vdots & \ddots & \vdots\vdots \\ a_{l1} & a_{l2} & \ldots & a_{lk}1 \end{bmatrix} * \begin{bmatrix} \text{IMF}_1 \\ \vdots \\ \text{IMF}_k \\ r(n) \end{bmatrix}, \quad (8)$$

where $\boldsymbol{a}_i = [\, a_{i1}\ a_{i2}\ \ldots\ a_{ik}1\,]$ $(i = 1, \ldots, l)$ represents the weight coefficient vectors of each IMF contributing to the reconstructed temperature, l is the number of weight coefficient vectors. The weight coefficients are built as the combination of the value from [0,1] with a step of 0.1 for each a_{ij}. For a signal with 5 IMFs, the number of weight coefficient vectors is $11^5 = 161051$. Since the procedure is parallel, the computation burden can be tremendously reduced when using an appropriate calculation platform.

Step 3 Choose optimized temperature $\text{new}(n)$ from $\text{new}_i(n)$ under the continuity constraint p_i $(i = 1, \ldots, l)$, which is defined by the maximum of the absolute value of two-order difference:

$$p_i = \max\left(\left|\frac{\text{new}_i(n-2) + \text{new}_i(n) - 2 * \text{new}_i(n-1)}{2}\right|\right), \quad 2 < n < N. \quad (9)$$

The smallest value of p_i means the best temperature continuity. Furthermore, we adopt a similarity constraint c_i to ensure the minimal deviation between the optimized temperature and the original temperature:

$$c_i = \frac{\sum_n (\text{origin}(n) - \overline{\text{origin}(n)})(\text{new}_i(n) - \overline{\text{new}_i(n)})}{\sqrt{\sum_n (\text{origin}(n) - \overline{\text{origin}(n)})^2 \sum_n (\text{new}_i(n) - \overline{\text{new}_i(n)})^2}}, \quad (10)$$

where $\overline{\text{origin}}$ and $\overline{\text{new}_i}$ denote the average temperatures of $\text{origin}(n)$ and $\text{new}_i(n)$, respectively.

Then the question of finding the optimized temperature $\text{new}(n)$ is equivalent to solving the following problem:

$$\text{new}(n) = \underset{\text{new}_i(n)}{\arg\min}\{p_i\} \cap \underset{\text{new}_i(n)}{\arg\max}\{c_i\}. \quad (11)$$

Step 4 Repeat Steps 1–3 on each row/column to yield the final optimized temperature image.

2.2.3. Quality assessment

The overshoot artifacts reflect the overshoot of temperature around the boundary, which is not correct in physics. Using the same method as in our previous study,[31] we take the mean variation of adjacent values from optimized temperature image as an evaluation criterion, which is defined as

$$\overline{\nabla T_i} = \frac{\sum_p \sum_{j=1}^{n_{i,p}-1} \left| T_{i,p,j} - T_{i,p,j+1} \right|}{\sum_p (n_{i,p} - 1)}, \tag{12}$$

where $n_{i,p}$ is the length of the p-th overshoot part in the i-th row/column, $T_{i,p,j}$ is the temperature of the j-th value in the p-th overshoot part in the i-th row/column. The mean variation of temperature of adjacent values in the whole image is given by

$$\overline{\nabla T} = \frac{\sum_i \sum_p \sum_{j=1}^{n_{i,p}-1} \left| T_{i,p,j} - T_{i,p,j+1} \right|}{\sum_i \sum_p (n_{i,p} - 1)}. \tag{13}$$

3. Experiment and analyses

Application of our proposed method to the abnormal data (marked by the red curve in Fig. 1) yields a satisfactory result as shown in Fig. 1 (marked by the green curve in Fig. 1). It can be clearly noticed that the overshoot artifacts in the mixture area significantly decreased. The mean variation between the rebuilt temperature and ground truth in the overshoot area is 0.2908 °C, while the mean variation is 1.9284 °C before applying our proposed method. In our phantom experiment, we use a cylindrical gelatin with a flow tube at the center to mimic the cancerous and benign masses embedded in glandular tissue.[36] To record both reflected ultrasound energy and transmitted ultrasound energy, a clinical ultrasound ring array scanner for breast cancer diagnosis was built (Karmanos Cancer Institute, Detroit, MI, USA).[37,38] During the experiment, all ultrasound transducer elements emit signals with the fan beam toward the opposite side of the ultrasound ring sequentially. The reflection ultrasound signals and the transmission ultrasound signals of each element are recorded to build images with acoustic propagation properties.[36]

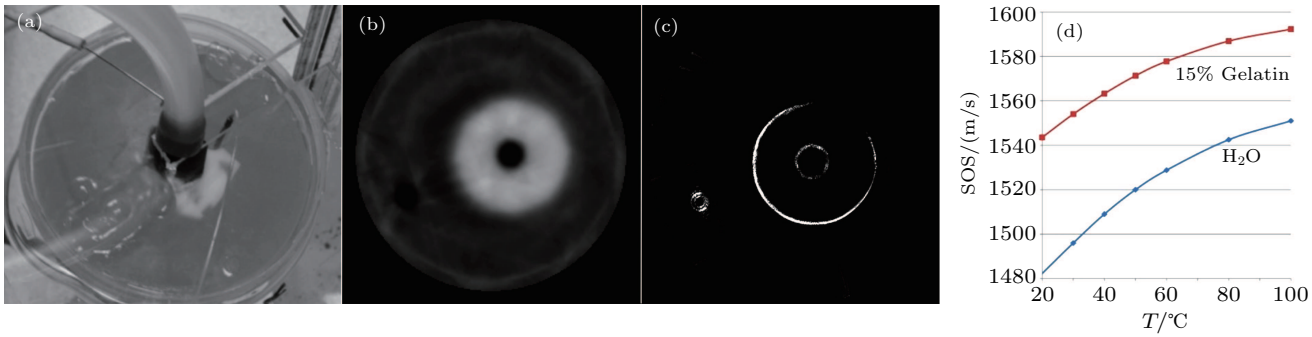


Fig. 2. (color online) Speed of sound imaging by a prototype SoftVue® breast imaging system. (a) Cylindrical phantom of gelatin immersed in water, with 15% gelatin (light cylinder with dark central hole from cooled water in thin walled latex tube) and with a very attenuating thick walled silicone flow return tube outside the gelatin at the 8 o'clock position; (b) speed of sound image; (c) reflection mode ultrasound image; (d) profiles of speed of ultrasound versus temperature for water and gelatin.

Reflection mode ultrasound image (Fig. 2(c)) and speed of sound images (Fig. 2(b)) of a cylindrical gelatin with a flow tube in the center immersed in water (Fig. 2(a)) are calculated by a prototype SoftVue®breast imaging system (Delphinus Medical Technologies, Inc., Plymouth, MI). The different sections of the image are segmented from reflection images. Curves of speed of sound vs. temperature of water and 15% gelatin are drafted from corresponding data in the literature[39,40] to yield the profiles (Fig. 2(d)).

Table 1. Mean temperature variation in different angles.

Angle/(°)	30	45	60	120	135	150
$\overline{\nabla T}_{\text{after}}$/°C	0.372	0.3773	0.3729	0.3860	0.3988	0.3795
$\overline{\nabla T}_{\text{original}}$/°C	0.922	0.879	0.8866	0.8880	0.8996	0.8981
$\overline{\nabla T}_{\text{pre_method}}$/°C	0.491	0.322	0.394	0.478	0.480	0.440

From the original un-optimized three-dimensional (3D) temperature (Fig. 3(a)) it follows that in the boundary between water and gelatin, there exist non-physical overshoot artifacts. Since the overshoot artifacts are not physically existing, the temperature profiles after optimization will apparently differ from the un-optimized temperature profiles. The result from the method based on our previous physical model is shown in Fig. 3(b). With our proposed method in this paper, the optimized 3D temperature image is shown in Fig. 3(c). The artifacts are obviously depressed and temperature in the mixture area is effectively optimized by both methods. The profiles of temperature and mean temperature variations of all image rows are compared in Figs. 3(d) and 3(e), respectively, showing almost the same optimization results and quality. The reduction of mean variation of temperature indicates that the overshoot artifacts are effectively eliminated and the smoothness of the mixture area is recovered. The mean temperature

variations in all rows and all columns decrease from 0.6845 °C to 0.2760 °C and 0.6893 °C to 0.2685 °C respectively after applying our optimized method. Since precisely monitoring the temperature is of great importance for insuring safe medical treatment, like the result in the numerical simulation, the absolute mean variation also effectively decreases, which increases the precision of the rebuilt temperature image. When calculating at six other angles (results are shown in Table 1), the image optimization results are close. Thus, we need not use BEMD (Bi-dimensional Empirical Mode Decomposition) to optimize the image.

When our previous method is applied, the temperature distribution of the mixture area is calculated by the finite element method with using Comsol®Multi-Physics 3.5a with 25 repeated iterations and temperature of the other area is also calculated. The total calculation time is over 5 minutes when using an 8-core Intel® X5570 HP XW8600 workstation with 64-GB memory. In addition, for comparison, the temperature field of the whole area optimized with the current method is also computed using an nVidia® Quadro K5200 GPU card since it contains no iteration. The total calculation time is less than 400 mil-seconds, which proves the advantages in reducing the computation burden with our proposed method in this paper. Furthermore, the whole optimization and reconstruction procedure is characterized with an adaptive property, which does not need any prior information or assumption.

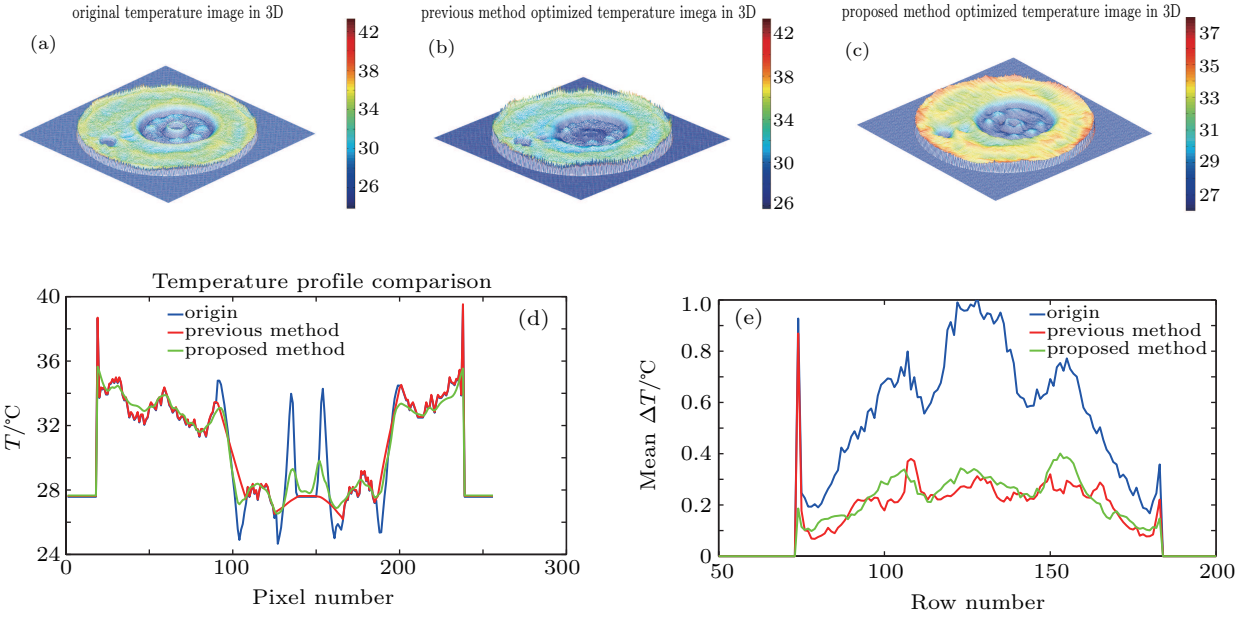


Fig. 3. (color online) Temperature images and comparisons. (a) Original 3D map of temperature from the segmentation of the speed of sound image using the reflection image; (b) temperature image from our previous method; (c) temperature image from our proposed method; (d) comparison among temperature profiles; (e) comparison among temperature mean variations.

4. Conclusions

Empirical mode decomposition is an excellent data analysis method for non-stationary signals with adaptive property. Signals reconstructed from IMFs with different weights can prevail favorably over those from a complicated filter. Here in this paper, our adopted EMD approach combined with similarity constraint and continuity constraint, can yield better optimization temperature images adaptively with less computation time than our previously proposed method. The phantom in this study mimics the cancerous and benign masses embedded in glandular tissue of human breast. In future human clinical study, temperature imaging through ultrasound transmission tomography for localized feedback of hyperthermia can present the more precise details to enhance the feasibility with acceptable computation time when stable ultrasound transmission tomography is applied.

Acknowledgement

We thank Neb Duric, the Karmanos Cancer Institute, Detroit and Delphinus Medical Technologies, LLC, Plymouth, MI and M L Scarpelli, University of Michigan students for contributions to conceptualization and for conducting the experiments, respectively.

References

[1] Falk M and Issels R 2001 *Int. J. Hyperther* **17** 1
[2] Kumar C S and Mohammad F 2011 *Adv. Drug. Del. Rev.* **63** 789
[3] Wust P, Hildebrandt B, Sreenivasa G, Rau B, Gellermann J, Riess H, Felix R and Schlag P M 2002 *Lancet. Oncol.* **3** 487
[4] Hildebrandt B, Wust P, Ahlers O, Dieing A, Sreenivasa G, Kerner T, Felix R and Riess H 2002 *Crit. Rev. OncolHematol* **43** 33
[5] Zagar T M, Oleson J R, Vujaskovic Z, Dewhirst M W, Craciunescu O I, Blackwell K L, Prosnitz L R and Jones E L 2010 *Int. J. Hyperther.* **26** 612
[6] Huilgol N G, Gupta S and Sridhar C R 2010 *J. Cancer Res. Ther.* **6** 492
[7] Cherukuri P, Glazer E S and Curley S A 2009 *Adv. Drug. Del. Rev.* **62** 339

[8] Issels R D, Lindner L H, Verweij J, Wust P, Reichardt P, Schem B C, Abdelrahman S, Daugaard S, Salat C andWendtner C M 2010 *Lancet. Oncol.* **11** 561

[9] Fessenden P, Lee E R and Samulski T V 1984 *Cancer Res.* **44** 4799s

[10] Dickinson R J, Hall A S, Hind A J and Young I R 1986 *J. Comput. Assisted Tomogr.* **10** 468

[11] Todd N, Vyas U, Bever J D, Payne A and Parker D L 2012 *Magn. Reson. Med.* **67** 724

[12] Daniels M J, Varghese T, Madsen E L and Zagzebski J A 2007 *Phys. Med. Biol.* **52** 4827

[13] Anand A, Savéry D and Hall C 2007 *IEEE T. Ultrason. Ferr.* **54** 23

[14] Maruyma K, Mizushina S, Sugiura T and Leeuwen G M J V 2000 *IEEE T. Microw. Theory* **48** 2141

[15] Le B D, Delannoy J and Levin R L 1989 *Radiology* **171** 853

[16] Ishihara Y, Calderon A, Watanabe H, Okamoto K, Suzuki Y, Kuroda K and Suzuki Y 1995 *Magn. Reson. Med.* **34** 814

[17] Diakite M, Odéen H, Todd N, Payne A and Parker D L 2014 *Magn. Reson. Med.* **72** 178

[18] Leroy Y, Bocquet B and Mamouni A 1998 *Physiol. Meas.* **19** 127

[19] Rahimian S and Tavakkoli J 2012 *J. Acous. Soc. Am.* **131** 3211

[20] Bamber J C and Hill C R 1979 *Ultrasound Med. Biol.* **5** 149

[21] Maass-Moreno R and Damianou C A 1996 *J. Acous. Soc. Am.* **100** 2514

[22] Maass-Moreno R, Damianou C A and Sanghvi N T 1996 *J. Acous. Soc. Am.* **100** 2522

[23] Arthur R M, Straube W L, Starman J D and Moros E G 2003 *Med. Phys.* **30** 1021

[24] Liu D and Ebbini E S 2010 *IEEE Trans. Biomed. Eng.* **57** 12

[25] Opieliński, Pruchnicki K J, Gudra P, Podgórski T, Kraśnicki P, Kurcz T, Sąsiadek J and Marek 2016 *Arch. Acoust.* **38** 321

[26] Miller N R, Bamber J C and Meaney P M 2002 *Ultrasound Med. Biol.* **28** 1319

[27] Shih T C, Yuan P, Lin W L and Kou H S 2007 *Med. Eng. Phys.* **29** 946

[28] Yang D, Converse M C, Mahvi D M and Webster J G 2007 *IEEE Trans. Biomed. Eng.* **54** 1382

[29] Krishnamoorthy R T S A R R M 2015 *Adv. Nat. Appl. Sci.* **9** 29

[30] Perrone D, Aelterman J, Pižurica A, Jeurissen B, Philips W and Leemans A 2015 *NeuroImage* **120** 441

[31] Chu Z Q, Yuan J, Pinter S Z, Kripfgans O D, Wang X D, Carson P L and Liu X J 2015 *Chin. Phys. B* **24** 104303

[32] Huang A N E 2001 *Int. Soc. Opt. Photon.* **2001** 71

[33] Huang N E, Shen Z, Long S R, Wu M C, Shih H H, Zheng Q, Yen N C, Chi C T and Liu H H 1998 *P. Roy. Soc. A-Math. Phys.* **454** 903

[34] Wu Z and Huang N E 2004 *P. Roy. Soc. A-Math. Phys.* **460** 1597

[35] Flandrin P, Rilling G and Goncalves P 2004 *IEEE Signal Proc. Lett.* **11** 112

[36] Li C, Duric N, Littrup P and Huang L 2009 *Ultrasound Med. Biol.* **35** 1615

[37] Duric N, Littrup P, Poulo L, Babkin A, Pevzner R, Holsapple E, Rama O and Glide C 2007 *Med. Phys.* **34** 773

[38] Li C, Duric N and Huang L 2008 *International Conference on Biomedical Engineering and Informatics* **2** 708

[39] Grosso V A D and Mader C W 1972 *J. Acous. Soc. Am.* **52** 1442

[40] Parker N G and Povey M J W 2012 *Food Hydrocolloid* **26** 99